INTERNATIONAL JOURNAL FOR NUMERICAL METHODS IN FLUIDS
Int. J. Numer. Meth. Fluids 2003; **42**:717–740 (DOI: 10.1002/fld.550)

Numerical simulation of turbulent flow through series stenoses

T. S. Lee*,†, Wei Liao and H. T. Low

Department of Mechanical Engineering, National University of Singapore, Singapore 119260

SUMMARY

The flow fields in the neighbourhoods of series vascular stenoses are studied numerically for the Reynolds numbers from 100 to 4000, diameter constriction ratios of 0.2–0.6 and spacing ratios of 1, 2, 3, 4 and ∞. In this study, it has been further verified that in the laminar flow region, the numerical predictions by k–ω turbulence model matched those by the laminar-flow modelling very well. This suggests that the k–ω turbulence model is capable of the prediction of the laminar flow as well as the prediction of the turbulent stenotic flow with good accuracy. The extent of the spreading of the recirculation region from the first stenosis and its effects on the flow field downstream of the second stenosis depend on the stenosis spacing ratio, constriction ratio and the Reynolds number. For $c_1 = 0.5$ with $c_2 \leqslant c_1$, the peak value of wall vorticity generated by the second stenosis is always less than that generated by the first stenosis. However, the maximum centreline velocity and turbulence intensity at the second stenosis are higher than those at the first stenosis. In contrast, for $c_1 = 0.5$ with $c_2 = 0.6$, the maximum values at the second stenosis are much higher than those at the first stenosis whether for centreline velocity and turbulence intensity or for wall vorticity. The peak values of the wall vorticity and the centreline disturbance intensity both grow up with the Reynolds number increasing. The present study shows that the more stenoses can result in a lower critical Reynolds number that means an earlier occurrence of turbulence for the stenotic flows. Copyright © 2003 John Wiley & Sons, Ltd.

KEY WORDS: series stenoses; turbulence; recirculation; numerical modelling

1. INTRODUCTION

The occurrence of turbulence in the arteries has long been realized [1]. The typical Reynolds number range of blood flow in the human body varies from 1 in small arterioles to approximately 4000 in the largest artery, the aorta [2]. In the absence of stenosis, the blood flow is usually laminar since the fully developed pipe flow does not experience transition to turbulence until the Reynolds number based on diameter and average flow speed exceeds about 2300. However, the obstruction presented by moderate and severe stenosis can lead to a highly disturbed flow region at the downstream of the stenosis. These disturbed flows may either remain laminar or undergo transition to turbulent flow, depending upon the specific flow conditions through the stenosis and the geometry of the stenosis.

*Correspondence to: T. S. Lee, Department of Mechanical Engineering, National University of Singapore, 10 Kent Ridge Crescent, Singapore 119260.
†E-mail: mpeleets@nus.edu.sg

Received 26 May 2002
Revised 6 January 2003

Turbulence represents an abnormal flow condition in the circulation and thus the development of turbulent flow has important clinical consequences. Numerous experimental studies for the steady turbulent flow in arteries have been carried out by many researchers, such as Clark [3], Deshpande *et al.* [4] and Saad *et al.* [5]. Deshpande *et al.* [4] performed the measurements of turbulent flow through a stenotic tube with a contoured 75% stenosis for a range of relatively high Reynolds number from 5000 to 15 000 with a laser Doppler anemometer. These studies have shown that the transitional flow or turbulence can be expected even in the artery with mild stenosis.

Numerical simulation of the stenotic flow offers a non-invasive means of obtaining detailed flow characteristics which are sometimes very difficult to obtain experimentally, such as wall shear stress distributions. The blood flow in the arteries mainly lies in the low Reynolds number range. Under this flow condition, it is more often seen that the turbulent, laminar and transitional regions coexist in the same stenotic flow field commonly with large separation bubble. As Wilcox [6] pointed out, the blood flow through the arterial stenosis is particularly difficult to simulate among the various separated-flow applications. Actually, most numerical simulations of stenotic flow have been confined to laminar flows with low Reynolds numbers. Deshpande [7] numerically predicted the turbulent flow in arterial stenosis with very high Reynolds number up to 15 000. In fact, however, such high Reynolds numbers are unrealistic when the human circulatory system is considered. Ghalichi *et al.* [8] presented the numerical results for the transitional and turbulent flow through the moderated and severe arterial stenosis over a range of physiologically relevant Reynolds number from 50 to 2000 using the FIDAP finite element software. It was established that the laminar flow model overestimated the vortex length when the flow becomes transitional or turbulent. Ghalichi *et al.* [8] used the Wilcox's standard version of the k–ω turbulence model [9] that is different from the Wilcox's low Reynolds number version of the k–ω turbulence model [10] although it was claimed that the low Reynolds number k–ω turbulence model was used. Ghalichi *et al.* [8] drew the conclusion that the Wilcox's k–ω turbulence model is suitable for blood flow studies in certain areas of the arteries where both laminar and transitional/turbulent flows coexist.

Multiple stenoses in diseased vascular tube may occur because of the formation of the primary stenosis that can result in downstream circulation flow. The downstream circulation in time will accumulate particles and forms a secondary stenosis. As a result of the secondary stenosis, a circulation zone will form at its downstream, thus resulting in a third stenosis, etc. The effects of these stenoses result in a series of sequence constrictions. An initial study through double stenoses was presented by Lee [11, 12] just for the laminar flows. Damodaran *et al.* [13] also numerically researched the steady laminar flows through the multiple constrictions in tubes for a range of Reynolds number 50–250. To our knowledge, however, none have considered the turbulent flows through the series stenoses.

The turbulent flow in a tube with axisymmetric stenosis is of great interest because of its relation to human vessels and the possibility of diagnosing the stenosis in its earlier stages. In the present study, a detailed analysis on the dynamics of the flow in a tube with double bell-shaped stenoses was presented with the relatively low Reynolds numbers from 100 to 4000 considered. Actually, it is realistic to consider the Reynolds numbers less than 4000 when the human arterial flows are simulated. The primary effort is to provide a comprehensive treatment for the steady flows through the realistically shaped stenoses by obtaining flow field solutions at various Reynolds numbers to ensure that the full range of turbulent flow is covered for the arterial flow. The dynamics of the flow describing separation, reattachment,

the formation of recirculation eddy and the distribution of the turbulent kinetic energy are revealed.

In the present work, the stenotic flow fields in an arterial tube was simulated numerically using the method which had been developed and validated in Lee *et al.* [14, 15] for solving the steady and unsteady incompressible Navier–Stokes equations and k–ω turbulence model equations in a two-dimensional, curvilinear co-ordinate system. Compared with the k–ω turbulence model, the K–ε model is easier to integrated through viscous sublayer since it does not require any additional low Reynolds number damping functions. The model equations are mathematically simpler and less stiff near the walls. From the point of computational implementation, therefore, this model appears especially attractive. More importantly, it has been designed to achieve more accurate predictions for adverse pressure gradient flows [6].

2. GOVERNING EQUATIONS AND NUMERICAL METHODS

As shown in Lee *et al.* [14, 15], the artificial compressibility approach presented by Chorin [16] initially just for steady flow has been developed to solve both steady and unsteady laminar and turbulent flows. In the present study, the artificial compressibility method was only used to solve steady turbulent flows. This involved modifying the governing equations to make them fully hyperbolic by adding an unsteady term to the mass conservation equation. The steady-state solution is not altered by modifying the equations in this way. Basing on Boussinesq's hypothesis, for axially symmetric flow of incompressible and Newtonian fluids, the Reynolds-averaged Navier–Stokes (RNS) equations with the modification of artificial compressibility can be written as

$$\frac{1}{\beta}\frac{\partial p}{\partial t} + \frac{\partial (ru)}{\partial z} + \frac{\partial (rv)}{\partial r} = 0 \tag{1a}$$

$$\frac{\partial (ru)}{\partial t} + \frac{\partial (ru^2)}{\partial z} + \frac{\partial (ruv)}{\partial r} = -\frac{\partial (rp)}{\partial z} + \frac{\partial}{\partial z}\left(r(v+v_t)\frac{\partial u}{\partial z}\right) + \frac{\partial}{\partial r}\left(r(v+v_t)\frac{\partial u}{\partial r}\right) \tag{1b}$$

$$\frac{\partial (rv)}{\partial t} + \frac{\partial (ruv)}{\partial z} + \frac{\partial (rv^2)}{\partial r} = -\frac{\partial (rp)}{\partial r} + \frac{\partial}{\partial z}\left(r(v+v_t)\frac{\partial v}{\partial z}\right) + \frac{\partial}{\partial r}\left(r(v+v_t)\frac{\partial v}{\partial r}\right) + p - v\frac{v}{r} \tag{1c}$$

Here the co-ordinate variables (r, z) are defined in the cylindrical co-ordinate system; u and v are the velocity components in z and r directions, respectively. v_t is the non-dimensional turbulent eddy viscosity which can be evaluated by the turbulence model. β is an artificial compressibility parameter. In order to satisfy the divergence free condition, the continuity equation having a pseudo-compressibility term is always solved iteratively in time until the pseudo-compressibility term vanished. The whole set of differential equations are physically unbalanced until the steady state solution is reached.

When turbulent flows are considered, the governing equations of Wilcox's k–ω turbulence model, in which k and ω are the turbulence kinetic energy and specific dissipation rate,

respectively, are written as follows [6, 9]:

$$\frac{\partial(rk)}{\partial t}+\frac{\partial(ruk)}{\partial z}+\frac{\partial(rvk)}{\partial r}$$
$$=rv_tP_d+\frac{\partial}{\partial z}\left[r(v+\sigma_k v_t)\frac{\partial k}{\partial z}\right]+\frac{\partial}{\partial r}\left[r(v+\sigma_k v_t)\frac{\partial k}{\partial r}\right]-r\beta_k k\omega \tag{2a}$$

$$\frac{\partial(r\omega)}{\partial t}+\frac{\partial(ru\omega)}{\partial z}+\frac{\partial(rv\omega)}{\partial r}$$
$$=r\gamma_\omega P_d+\frac{\partial}{\partial z}\left[r(v+\sigma_\omega v_t)\frac{\partial \omega}{\partial z}\right]+\frac{\partial}{\partial r}\left[r(v+\sigma_\omega v_t)\frac{\partial \omega}{\partial r}\right]-r\beta_\omega \omega^2 \tag{2b}$$

Here

$$P_d=2\left[\left(\frac{\partial u}{\partial z}\right)^2+\left(\frac{\partial v}{\partial r}\right)^2+\left(\frac{v}{r}\right)^2\right]+\left(\frac{\partial u}{\partial r}+\frac{\partial v}{\partial z}\right)^2 \tag{3}$$

The eddy viscosity is calculated from

$$v_t=\frac{k}{\omega} \tag{4}$$

The closure coefficients for the k–ω turbulence model are

$$\beta_k=0.09,\quad \sigma_k=0.5,\quad \beta_\omega=0.075,\quad \sigma_\omega=0.5,\quad \gamma_\omega=5/9$$

In the numerical process, the Reynolds-averaged Navier–Stokes equations in the conservation form are usually non-dimensionalized and then expressed in a generalized curvilinear co-ordinate system with the axisymmetric physical components taken as the dependent variables as follows:

$$\frac{\partial W}{\partial t}+\frac{\partial E}{\partial \xi}+\frac{\partial F}{\partial \eta}=\frac{\partial E_V}{\partial \xi}+\frac{\partial F_V}{\partial \eta}+S \tag{5}$$

where

$$W=Jr\begin{bmatrix}p\\u\\v\end{bmatrix}$$

$$E=Jr\begin{bmatrix}\beta U\\uU+p\xi_z\\vU+p\xi_r\end{bmatrix},\quad F=Jr\begin{bmatrix}\beta V\\uV+p\eta_z\\vV+p\eta_r\end{bmatrix}$$

$$E_v=Jr\frac{1}{\mathrm{Re}}(1+v_t)\begin{bmatrix}0\\\alpha_1u_\xi+\alpha_2u_\eta\\\alpha_1v_\xi+\alpha_2v_\eta\end{bmatrix},\quad F_v=Jr\frac{1}{\mathrm{Re}}(1+v_t)\begin{bmatrix}0\\\alpha_2u_\xi+\alpha_3u_\eta\\\alpha_2v_\xi+\alpha_3v_\eta\end{bmatrix}$$

$$S = Jr \begin{bmatrix} 0 \\ 0 \\ \dfrac{p}{r} - \dfrac{1}{\mathrm{Re}}(1+v_t)\dfrac{v}{r^2} \end{bmatrix}$$

In the governing equations, J is the Jacobian of the transformation. U, V are contravariant velocities in ξ, η-direction given by

$$U = \xi_z u + \xi_r v$$
$$V = \eta_z u + \eta_r v$$

and

$$\alpha_1 = \xi_z^2 + \xi_r^2, \quad \alpha_2 = \xi_z \eta_z + \xi_r \eta_r, \quad \alpha_3 = \eta_z^2 + \eta_r^2$$

Similar to the Navier–Stokes equations, the k–ω turbulence model equations can also be non-dimensionalized and re-formulated in a generalized curvilinear co-ordinate system with the axisymmetric physical components taken as the dependent variables. It results in the following system of equations in conservation form:

$$\frac{\partial \tilde{W}}{\partial t} + \frac{\partial \tilde{E}}{\partial \xi} + \frac{\partial \tilde{F}}{\partial \eta} = \frac{\partial \tilde{E}_V}{\partial \xi} + \frac{\partial \tilde{F}_V}{\partial \eta} + \tilde{S} \tag{6}$$

where

$$\tilde{W} = Jr \begin{bmatrix} k \\ \omega \end{bmatrix}$$
$$\tilde{E} = Jr \begin{bmatrix} Uk \\ U\omega \end{bmatrix}, \quad \tilde{F} = Jr \begin{bmatrix} Vk \\ V\omega \end{bmatrix}$$
$$\tilde{E}_v = Jr \frac{1}{\mathrm{Re}} \begin{bmatrix} (1+\sigma_k v_t)(\alpha_1 k_\xi + \alpha_2 k_\eta) \\ (1+\sigma_\omega v_t)(\alpha_1 \omega_\xi + \alpha_2 \omega_\eta) \end{bmatrix}$$
$$\tilde{F}_v = Jr \frac{1}{\mathrm{Re}} \begin{bmatrix} (1+\sigma_k v_t)(\alpha_2 k_\xi + \alpha_3 k_\eta) \\ (1+\sigma_\omega v_t)(\alpha_2 \omega_\xi + \alpha_3 \omega_\eta) \end{bmatrix} \tag{7}$$
$$\tilde{S} = Jr \begin{bmatrix} v_t P_d - \beta_k k\omega \\ \gamma_\omega P_d - \beta_\omega \omega^2 \end{bmatrix}$$

$$P_d = 2\left[(u_\xi \xi_z + u_\eta \eta_z)^2 + (v_\xi \xi_r + v_\eta \eta_r)^2 + \left(\frac{v}{r}\right)^2\right] + (u_\xi \xi_r + u_\eta \eta_r + v_\xi \xi_z + v_\eta \eta_z)^2$$

Here the eddy viscosity is obtained from

$$v_t = \mathrm{Re}\,\frac{k}{\omega} \tag{8}$$

In Equations (5) and (6), the dimensionless variables $r^* = r/r_0$, $z^* = z/r_0$, $u^* = u/u_0$, $v^* = v/u_0$, $t^* = t/t_0$, $p^* = p/\rho u_0^2$, $k^* = k/u_0^2$ and $\omega^* = \omega r_0/u_0$ have been used and asterisks are dropped for

brevity. $\mathrm{Re} = r_0 u_0 / v$ is the Reynolds number. Here t_0 can be got as r_0/u_0; r_0 is the radius of the tube infinitely far upstream; u_0 is the inlet velocity. In deriving the equations, constant density were assumed for simplicity.

In the present study, the solution procedure is based on the method of artificial compressibility and uses a decoupled approach to solve the Reynolds-averaged Navier–Stokes equations and k–ω turbulence model equations. Michelassi *et al.* [17] pointed out that the coupled solver showed no improvement in convergence or accuracy in comparison with the decoupled approach. Furthermore, the decoupled approach will make it easier to select the suitable turbulence models according to the flows to be simulated without great modification for the code. In the current decoupled approach, the Reynolds-averaged Navier–Stokes equations are implicitly solved to update the pressure and the velocity field; then the k–ω model equations are solved together with the new given velocities to compute a new turbulent viscosity field. The above process is repeated until the convergence criterion is satisfied. The same algorithms can also be applied to solve both the Navier–Stokes equations and the k–ω model equations, including the discretization of the time, convective and diffusive terms. The lower–upper symmetric-Gauss–Seidel (LU-SGS) implicit algorithm is used as the time integration scheme for the governing equations because of its efficiency and stability. When constructing this scheme, the advantages of recent advances in CFD are taken into considerations. The LU-SGS method is applied with the use of upwind-biased and total variation diminishing (TVD) scheme. To calculate the convective flux, an edge-based method is used by calculating and storing the flux integrals based on edges. The convective fluxes are discretized by using the appropriate form of Roe's flux-difference splitting [15, 18]. The high-order upwind-biased monotonic upstream schemes for conservation laws (MUSCL) scheme with satisfying TVD conditions is used to deal with the convective terms, which shows evident advantage and is helpful to stabilize the computation and increase the convergent speed. This is because the steep gradients exist in the k, ω fields. In a typical profile of ω normal to the wall, the value of ω can vary rapidly from 10^5 (even the value is higher for finer grids) near the wall to 1 outside the boundary layer. Actually the high-resolution TVD scheme is just designed to deal with such large gradients. In order to obtain the solutions satisfying TVD conditions, the MINMOD limiter is herein introduced into the construction of MUSCL scheme. The viscous terms are evaluated by the second-order central difference. The details and validation of the current numerical method for incompressible flows can be found in Lee *et al.* [14, 15].

The artificial compressibility parameter β influences both the accuracy and the efficiency of the calculation. However, it is easy to find a range of β for which the code would converge very quickly. As has been referred to in Lee *et al.* [14, 15], the current scheme was found not to be sensitive to the value of the artificial compressibility parameter and the present code is stable for a wide range of β. In the present study, a constant value of the parameter β has been used. For all cases, the value of β is set to 1 that was found to give a good rate of convergence and accuracy for all of the problems considered.

3. GEOMETRY AND BOUNDARY CONDITIONS

In the present study, the steady turbulent flows through single or series stenoses are dealt with. The geometrical configuration of the vascular tube with double stenoses with its co-ordinate system is shown in Figure 1.

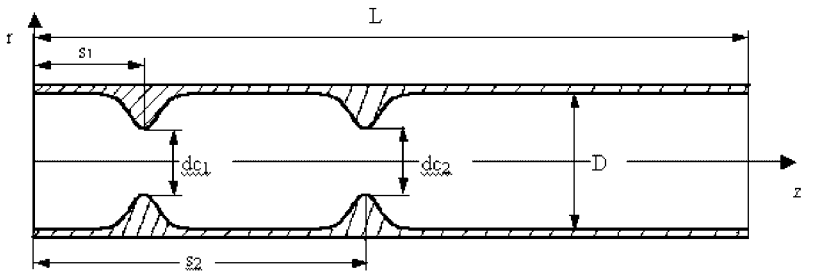

Figure 1. Stenosis geometry used in the steady turbulent flow analysis.

As shown in Figure 1, L is the length of the tube under consideration; D is the diameter of the tube having a constant cross section; d_c is the opening of the constriction; s_1, s_2 are distances of the first and second stenosis from inlet plane, respectively; and S is the spacing between stenoses, $S=(s_2-s_1)$.

The geometry of the stenosis may be described by the following bell-shaped Gaussian distribution profile [11]:

$$f(z)=1-c_i\exp(-c_s(z-s_i)^2) \tag{9}$$

where c_i is constriction ratio $(D-d_{ci})/D$; c_s is a shape constant; z_1, z_2 are limits of the first constriction and z_3, z_4 are limits of the second constriction. c_1 is the upstream stenosis constriction ratios defined as $c_1=(D-d_{c1})/D$; c_2 is the downstream stenosis constriction ratios defined as $c_2=(D-d_{c2})/D$. In the present study, the constriction ratios c_1 and c_2 were always less than 1 and c_s was fixed at 4.0.

The double bell-shaped stenosed tube was translated into a rectangular solution domain in a curvilinear co-ordinate system. The boundary types encountered in the present study were classified as inflow, outflow, solid wall and symmetrical plane. As done in Lee *et al.* [14, 15], all boundary conditions were imposed using ghost cells that are two rows of fictitious cells next to the boundary. With this concept the boundary fluxes were treated in a fashion similar to the internal fluxes.

At the inflow boundary, the non-dimensional velocities were specified by

$$u_{\text{in}}=1-r^2, \quad v_{\text{in}}=0 \tag{10}$$

The pressure was extrapolated from the interior. k and ω in non-dimensional form were set at very low levels at the inflow because the flows only with relatively low Reynolds numbers were considered in this study

$$k_{\text{in}}=1.5I_{\text{T}}^2u_{\text{in}}^2, \quad \omega_{\text{in}}=\frac{\sqrt{k_{\text{in}}}}{C_\mu^{1/4}l_{\text{in}}} \tag{11}$$

where I_{T} is the turbulence intensity, usually taken to be 1%, $C_\mu=0.09$ and l_{in} is the length scale given by

$$l_{\text{in}}=\min(\kappa y_{\text{wall}}, 0.1R_0) \tag{12}$$

Here y_{wall} is the normal distance from the wall and $\kappa=0.41$ denotes the universal von Karman constant. For internal flows, at the outflow boundary the velocities were extrapolated from

the interior and a constant static pressure was imposed. The streamwise gradients of k and ω were assumed zero at exit, i.e.

$$\frac{\partial k}{\partial z} = \frac{\partial \omega}{\partial z} = 0 \tag{13}$$

On a solid surface, the usual no-slip condition was applied. The pressure at the wall was obtained by setting the gradient of the pressure equal to zero at the no-slip wall. The non-slip wall boundary conditions for the k–ω model equations were

$$k = 0, \quad \omega = \frac{6v}{\beta_\omega y_l} \tag{14}$$

Along the axis of symmetry, the gradients of k and ω in r-direction were assumed zero, i.e.

$$\frac{\partial k}{\partial r} = \frac{\partial \omega}{\partial r} = 0 \tag{15}$$

4. VALIDATION OF NUMERICAL METHOD

The computational results for two test problems are presented to verify the accuracy of the method. The performance of the present model is evaluated by comparing the results with the experimental data or numerical results of other researchers.

4.1. Fully developed steady channel flow

The first case chosen to assess the numerical implementation of the current turbulence model is a fully developed channel flow at $\mathrm{Re}_H = 13\,750$, for which turbulence quantities are available from the direct numerical simulation (DNS) data presented by Mansour *et al.* [19]. The Reynolds number Re_H is based on channel height and the average inlet velocity. The computation is performed on a non-uniform grid of 161×41. The cell centres closest to the wall surface lies below $y^+ = 1$ from the wall. The calculated velocity profiles in the turbulent boundary layer are displayed in Figure 2.

In Figure 2(a) and 1(b), an excellent agreement is observed between current velocity profiles with the DNS data and wall functions. The wall functions include the theoretical linear sublayer law

$$u^+ = y^+ \quad (0 \leqslant y^+ \leqslant 5) \tag{16}$$

and the theoretical logarithmic law of the wall

$$u^+ = \frac{1}{\kappa} \log\, y^+ + 5.1 \quad (30 \leqslant y^+ \text{ and } y < 0.1\delta) \tag{17}$$

Here $y^+ = yu_\tau/v$, $u^+ = u/u_\tau$.

4.2. Steady turbulent flow inside a circular tube with a constriction

This case deals with the steady turbulent flow inside a circular tube with a constriction. This flow has been studied experimentally by Deshpande *et al.* [4]. The geometry of the

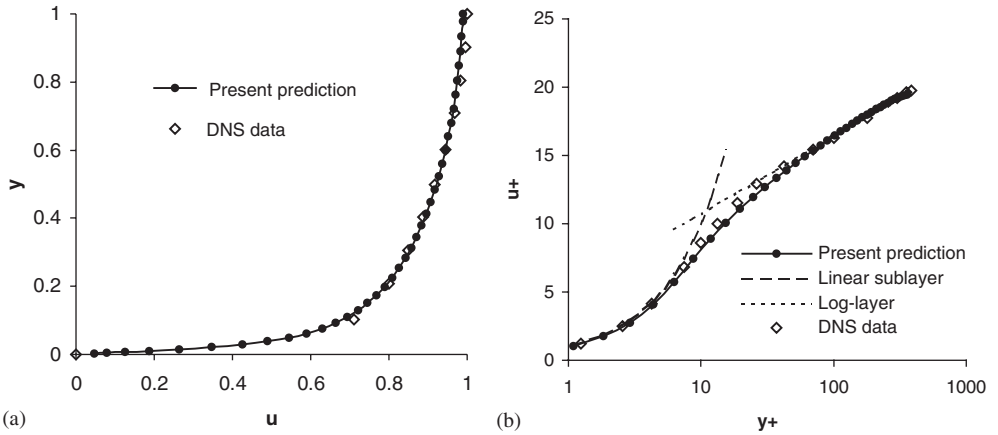

Figure 2. Comparison of the predicted velocity profiles and the DNS data (Mansour *et al.* [19]): (a) fully developed streamwise velocity profiles; (b) velocity distribution in the viscous sublayer and in the logarithmic layer.

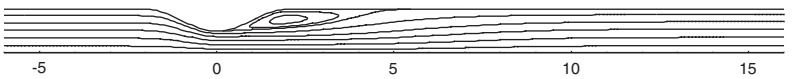

Figure 3. Streamlines for the turbulent flow through a constriction at Re = 15 000.

axisymmetric constriction may be described by the following profile:

$$\frac{r}{r_0} = 1 - \frac{\delta}{2r_0}\left(1 + \cos\frac{\pi z}{z_0}\right), \quad -z_0 \leqslant z \leqslant z_0 \tag{18}$$

In this case, $\delta = \frac{1}{2}r_0$, $z_0 = 2.0$ and the Reynolds number based on the diameter and the average inlet velocity is 15 000. Deshpande *et al.* [4] stated that the fully developed u-velocity profile is in reasonable agreement with the power law profile ($n \cong 6.4$) for Re = 15 000. So the velocity profile at the upstream inlet boundary is described by

$$u = u_0\left(1 - \frac{r}{r_0}\right)^{1/6.4}, \quad v = 0$$

where u_0 is the centreline velocity. At the inlet, the turbulence intensity I_T in Equation (11) is taken to be 3% [20].

The computational domain is extended from z-position $-6r_0$ to $16r_0$. Below presented are some results computed on a 201×41 grid, which gives sufficient resolution, as verified by mesh refinement. Figure 3 shows the geometrical shape of the computational domain and streamlines computed by the current method.

The computed separation and reattachment lengths are presented together with the experimental data of Ref. [4] and earlier calculations of Rastogi [21], Melaaen [22] and Zijlema *et al.* [20] in Table I. In fact, the separated point and reattachment point were not accurately measured by Deshpande *et al.* [4]. The corresponding value in Table I was from the estimation

Table I. Separation and reattachment locations.

	Separation, x_s/r_0	Reattachment, x_r/r_0
Deshpande *et al.* (Exp.)	$\approx 0.4-0.5$	≈ 4.0–4.5
Rastogi, 41×21	1.2	2.4
Melaaen, 52×22	0.56	4.067
Zijlema *et al.*, 150×100	0.56	3.50
Present, 201×41	0.41	4.35

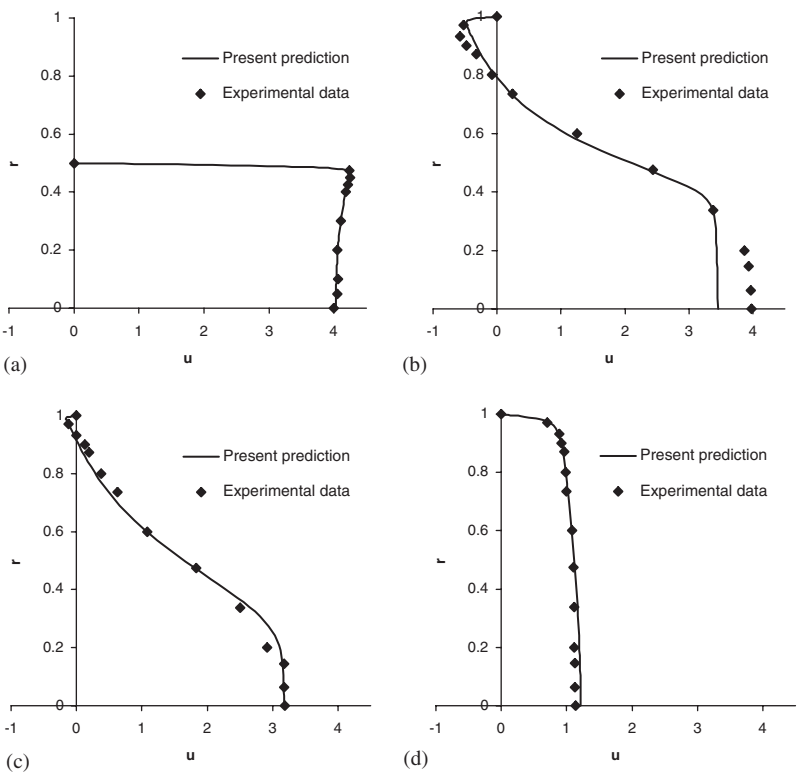

Figure 4. Comparison of computed and measured (Deshpande *et al.* [4]) axial velocity profiles at different axial positions: (a) $z = 0$; (b) $z = 2.5$ (c) $z = 4.0$; (d) $z = 11.0$.

according to the experimental velocity profiles of Ref. [4] as was done by Melaaen [22]. From Table I, it can be seen that the current method gives a recirculation zone in good accordance with the measurements.

Figures 4–6 present other typical features of this flow, including the streamwise velocity at different stations, centreline velocity and wall static pressure. The calculation is seen to yield very good agreement with the measurements. As shown in Figure 4, the streamwise velocity predictions fit the measurements of Ref. [4] very well, except for the station $z/r_0 = 2.5$. It is not surprising because it is well known that most turbulence models cannot scale well in and around the recirculation zone. The flow separates from the curved wall in the diverging part

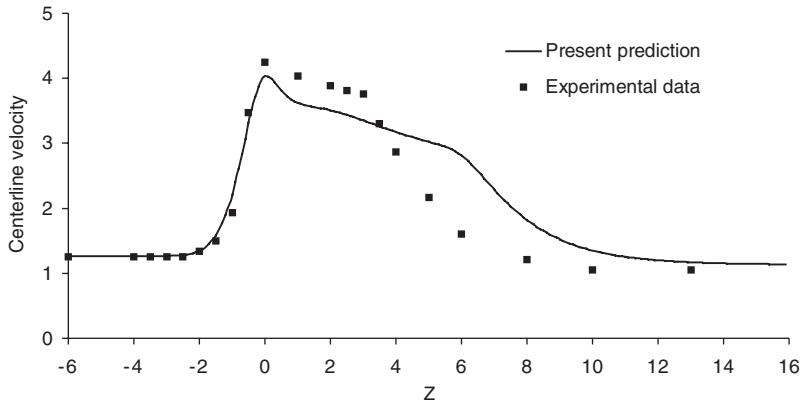

Figure 5. Distribution of the centreline velocity through the constriction (the experimental data originated from Deshpande *et al.* [4]).

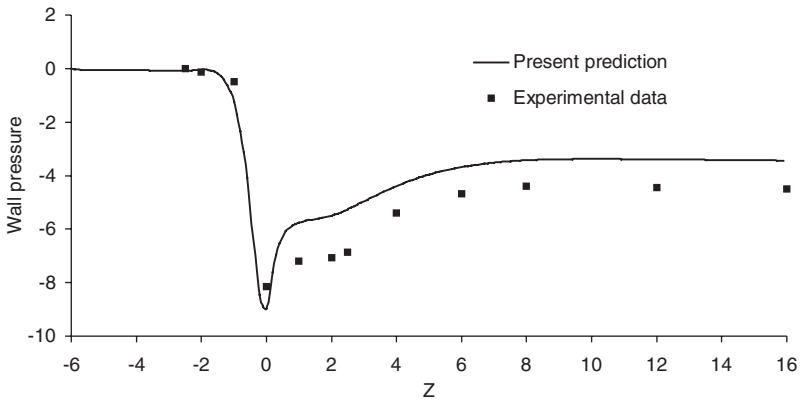

Figure 6. Distribution of the wall static pressure through the constriction (the experimental data originated from Deshpande *et al.* [4]).

of the constriction because the severe adverse pressure gradients occur there as the flow area increases and the fluid is greatly decelerated. The analogical situation can be found from the distribution of the centreline velocity in Figure 5 and wall static pressure in Figure 6, namely, the two distributions are not accurately predicted within the deceleration region compared with the experimental data. In fact, the present method has produced much closer velocity profiles and wall static pressure distribution than many other methods, such as Rastogi [21] and Zijlema *et al.* [20] and even a bit better than Melaaen [22] (see his Figure 22).

The comparison between current numerical results and the experimental data and computational results provided by other researchers illustrates that the current numerical solver is capable of simulating turbulent flows in the stenosed arteries, which are usually characterized by large recirculating vortex, with good accuracy and stability.

5. RESULTS AND DISCUSSION

It is well known that the blood flow in the arteries mainly lies in the low Reynolds number range. The time-average Reynolds number is approximately from 400 to 2000 for the large arteries in the human bodies. Without stenosis the flow is usually laminar since a fully developed pipe flow does not experience transition to turbulence until the Reynolds number based on diameter and average flow speed exceeds about 2300. However, the severe stenosis can lead to highly disturbed flow in the downstream of the stenosis. Whether the disturbed flows undergo transition to turbulent flow or remain laminar depends on the different flow conditions, such as the flow rate and the size of stenosis. In fact, the blood flow through the severe stenosis is a very complicated flow in which the large separated bubble will occur and furthermore the laminar, transitional and turbulent regions often coexist there. More importantly, when an unknown flow is to be predicted, often it is difficult to determine in advance whether the flow has become turbulence or not. In the simulation of the blood flow through stenosis, therefore, it should be necessary that the chosen turbulence model is capable of simulating both turbulent flow and laminar flow well. The k–ω turbulence model seemed to own this ability which was referred to by Ghalichi [8].

In the present study, the characteristics of the flows through the single and series stenoses were investigated. The geometrical configuration of the stenosis model used in this study has been shown in Figure 1. For all cases, the constriction ratio of the first stenosis was fixed to 0.5 that corresponds to a 75% area reduction. This percentage is critical in that the surgical treatment is often based on whether the coronary artery is more than 75% stenotic [2]. At first, the flows in a tube with single stenosis were considered with the Reynolds numbers varying from 100 to 4000 which are based on the radius of the tube having a constant cross section and the axial velocity at the inflow. The k–ω model's capability of simulating the laminar flow field was examined further. Then the turbulent flows through double stenoses in a tube were studied for various spacing ratios, Reynolds numbers and constriction ratios. The dynamics of the flows describing separation, reattachment, the formation of recirculation eddy and the distribution of the turbulent kinetic energy were revealed.

At the upstream inlet, there are not the known velocity profiles to be found for each Reynolds number. Therefore, the computational domain for single stenosis is extended with enough length from z-position $-15r_0$ to $20r_0$ with the centre of the stenosis located on zero position in order to eliminate the ill effects of inlet and outlet boundary conditions. A 201×41 grid, which is highly stretched in the height direction, is used in the cases with single stenosis and gives sufficient resolution as verified by mesh refinement. For the cases with double stenoses, the computational domain is further extended to ensure the length of $15r_0$ before the first stenosis and $20r_0$ behind the second stenosis, respectively. The grid number is also increased according to the distance between the double stenoses so as to ensure the same grid density in the z-direction as that for the cases with single stenosis. The rude computational grid in the tube with double stenoses is shown in Figure 7.

5.1. Low Reynolds number turbulence modelling through an arterial stenosis

In this study, the relatively low Reynolds numbers are considered with the values from 100 to 4000. The geometrical configuration of the stenosis model was the same as shown in Figure 1.

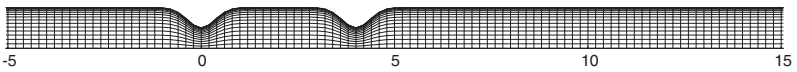

Figure 7. The (crude) computational grid in the tube with double stenoses.

In this case, the model only with one stenosis is considered. The constriction ratio of the first stenosis was set to 0.5 and that of the second stenosis was set to 0.

Figure 13 shows the streamlines of the flow through arterial stenosis for various Reynolds numbers that were predicted by the turbulence modelling. It can be seen that a circulation zone is formed behind the stenosis for all these Reynolds numbers. There is a separation streamline that divides the flow into two parts: the circulation flow field behind the stenosis and the main flow field near the centre of the tube with relatively straight and parallel streamlines. We know that the vortex length should increase with the Reynolds number increasing in the state of laminar flow until it reaches a critical peak value. Beyond the critical value, the flow becomes transitional or turbulent and the vortex length should decrease with Re increasing. From Figure 8, it can be seen that the vortex length for this size of stenosis reaches the maximum value around Reynolds number 300. Noting that the current Reynolds number is based on the radius of the tube and the upstream centreline velocity, we can deduce that this result is consistent with the experimental measurements by Yongchareon [23] that reported the transitional Reynolds number 400 based on the diameter of the tube and the upstream mean inlet velocity for a 75% stenosis.

Figure 9 presents the nature of the non-dimensional wall vorticity variation in the axial direction with different Reynolds numbers. The wall vorticity values, which are related to the velocity distribution, are of considerable interest to researchers because they are directly related to the wall shear stress in Newtonian flows. As shown in Figure 9, the magnitude of the wall vorticity value increases rapidly when the flow approaches the stenosis and reaches a peak value slightly upstream of the maximum stenosed area. Then the wall vorticity decreases rapidly and reverses to negative values at a location downstream of this peak value where separation starts at the wall of the tube. It is clearly observed that the peak wall vorticity value increases with Reynolds number increasing. The location of the peak wall vorticity values tends to shift upstream as the Reynolds number is increased and then keeps at about 0.2 radii upstream of the maximum stenosed area for relatively large Reynolds numbers. The negative wall vorticity values give an indication of the extent of the recirculation region in the stenosed flow. The negative magnitude of the wall vorticity value in the recirculation region also increases when the Reynolds number is increased.

The predicted wall pressure and centreline velocity distribution for $\mathrm{Re} = 100$ and 300 are plotted in Figure 10 in comparison with the results given by laminar-flow modelling. The computer code of laminar-flow modelling, which is just for the simulation of the laminar flow without the use of turbulence models, has been validated in Lee *et al.* [14] and proved to be a reliable tool for the numerical simulation of laminar flow. From Figure 10(a) and 10(b), it can be seen that in this case, k–ω turbulence model obtained the same numerical results as those obtained by the laminar-flow modelling for $\mathrm{Re} = 100$. For so low a Reynolds number, the flow is fully laminar. At the same time, for Reynolds number 300, the discrepancy between the results given by the two modelling can be found from Figure 10(a) and 10(b). Especially,

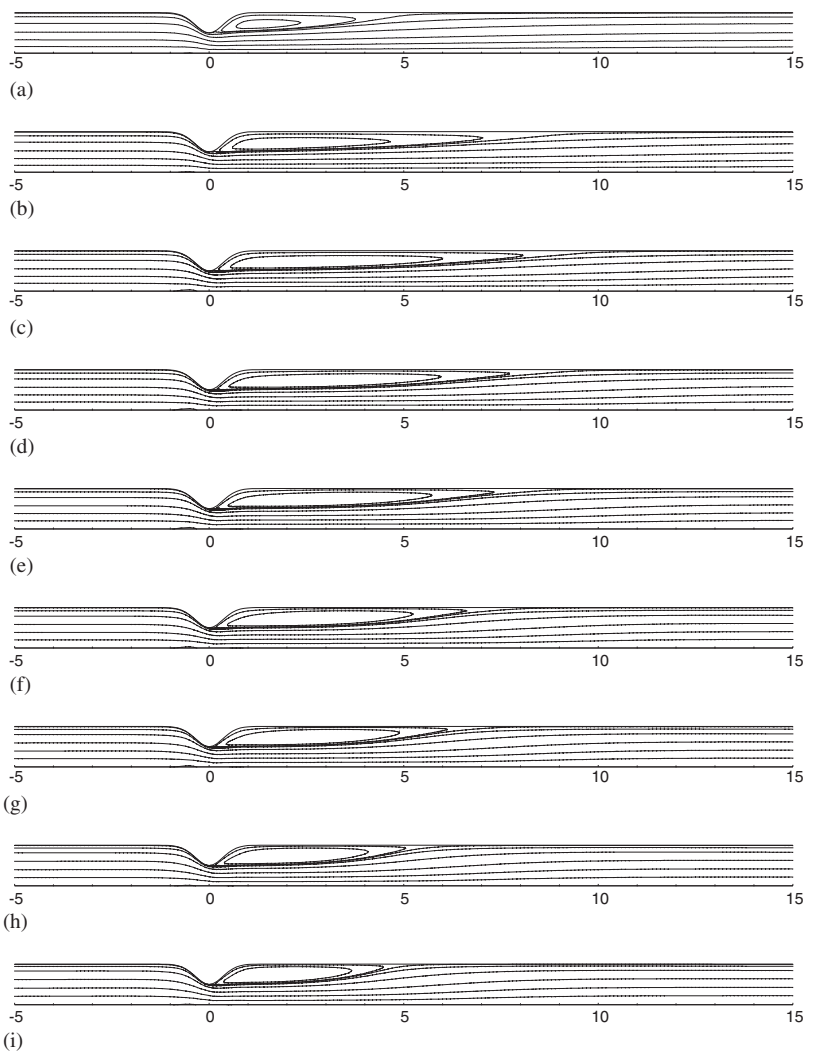

Figure 8. The streamlines of turbulent flows in the tube with single stenosis for the different Reynolds numbers from 100 to 4000: (a) Re = 100; (b) Re = 200; (c) Re = 300; (d) Re = 400; (e) Re = 500; (f) Re = 750; (g) Re = 1000; (h) Re = 2000; (i) Re = 4000.

Figure 10(b) shows that the laminar-flow modelling gives a much slower centreline velocity recovery prediction in the deceleration zone. As discussed above, this is because that the flow distal to the stenosis becomes transitional beyond the Reynolds number 300 and the laminar-flow modelling cannot simulate such flows properly. The laminar-flow modelling overestimated the vortex length distal to stenosis when the flow becomes transitional or turbulent. Therefore, it can be concluded that k–ω model can obtain the accurate numerical results even if the flow lies in the laminar flow range.

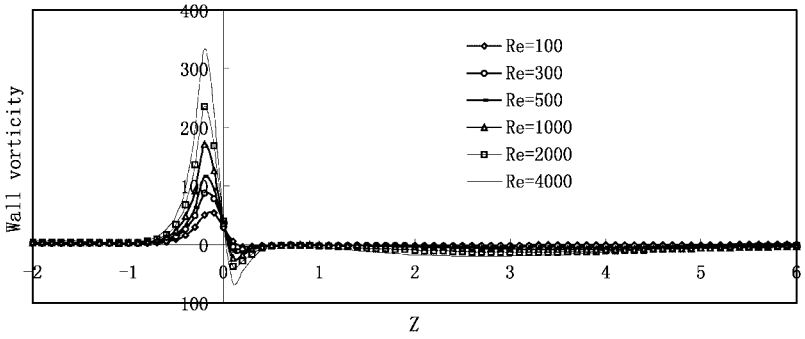

Figure 9. Wall vorticity distribution for different Reynolds numbers.

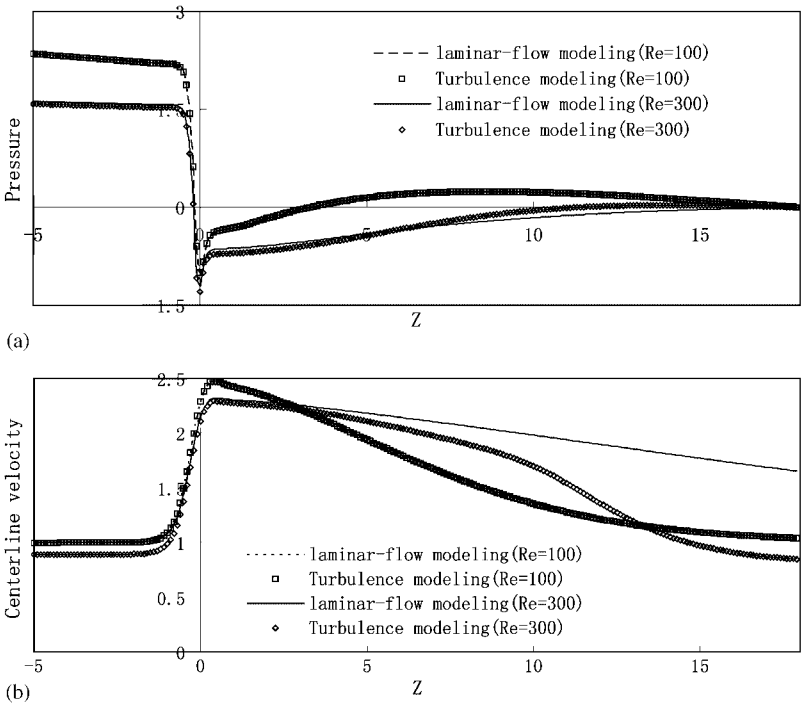

Figure 10. Comparison between the results by turbulence modelling and those by laminar-flow modelling: (a) wall static pressure distribution; (b) centreline velocity distribution.

5.2. The turbulent flows through series stenoses

Multiple stenoses in diseased vascular tube may occur because the formation of the primary stenosis may induce more stenoses to form in the downstream region. A study for the laminar flows through double stenoses was initially presented by Lee [11]. In the present work, the flow behaviour in a double stenosed symmetrical tube was studied numerically. The primary effort is to provide a comprehensive understanding for the characteristics of the turbulent

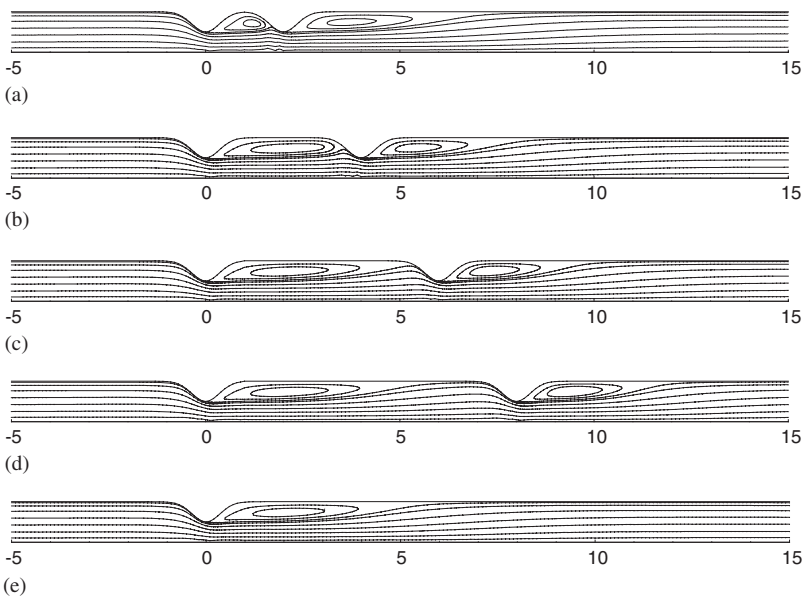

Figure 11. The streamlines of turbulent flows in the stenosed tube at different S/D for Reynolds number 2000: (a) $S/D = 1$; (b) $S/D = 2$; (c) $S/D = 3$; (d) $S/D = 4$; (e) $S/D = \infty$.

flow fields through the series stenoses. In this work, the flow fields in the neighbourhood of vascular stenoses in series were numerically studied in detail for different Reynolds number, spacing ratios and constriction ratios of the second stenoses. The dynamics of the flow, which describes the formation of recirculation eddy and distribution of the turbulent kinetic energy, were revealed by the streamline, velocity and pressure fields. The constriction ratio of the upstream stenosis in a tube was fixed at 0.5 while the downstream stenosis was allowed to vary from 0.2 to 0.6. The Reynolds number was allowed to vary from 100 to 4000 and the spacing ratio is considered from 1 to ∞. Actually, the spacing ratio $S/D = \infty$ corresponds to the case of a single stenosis in a tube.

At first, the behaviour of the recirculating flow region through the double stenoses was investigated for stenosis spacing ratios of 1 to ∞ with Reynolds number 2000. In this case, the constriction ratio of the second stenosis was also set to 0.5. The streamline distributions for this investigation are shown in Figure 11. From this figure, it can be observed that the recirculation eddies are formed downstream of each stenosis for different constriction spacing ratios. There exists a separation streamline that divides the flow into two regimes one of which is the recirculating region distal to each stenosis, and the other is the main flow field carrying the bulk of the flow near the centre of the tube. When S/D is less than 3, a recirculation zone fills the valley region between the two stenoses. The corresponding reattachment point is located on the front part of the second stenosis. Evidently, the development of the recirculation zone is restricted by the downstream stenosis. When S/D is larger than 3, a stable recirculation zone is established between the two stenoses and there is little change for the corresponding separation and reattachment points. This is because the valley region is enough large and has less limitation to the formation of the vortex. The size of the recirculation zone distal to the

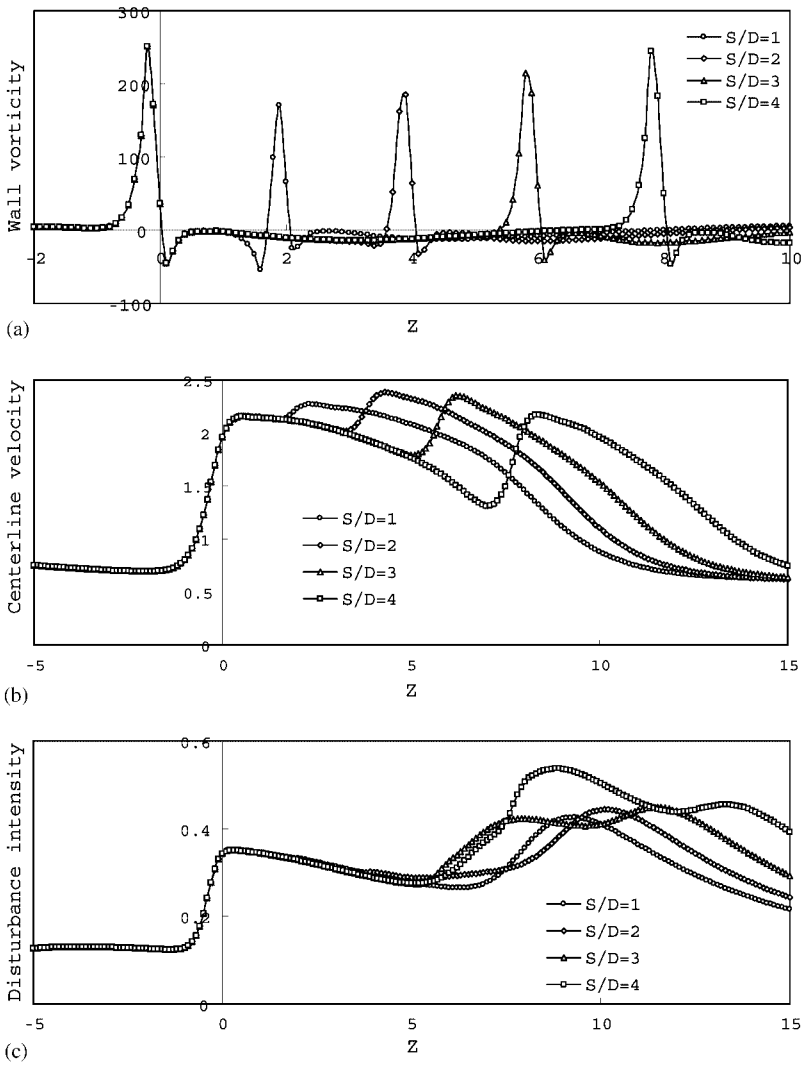

Figure 12. The flow characteristics through the double stenoses at different S/D for the Reynolds number 2000: (a) wall vorticity distribution; (b) centreline velocity distribution; (c) centreline disturbance intensity distribution.

second stenosis reduces with S/D increasing. For $S/D = 4$, the recirculation zone distal to the second stenosis is much smaller than that distal to the first stenosis. It can be inferred that the higher turbulence intensity occurs in the distal of the second stenosis which should be caused by the superposed effect of both stenoses. Therefore, the first stenosis has still an important impact on the flow fields near the second stenosis even if the spacing ratio S/D reaches 4.

Figure 12(a), 12(b) and 12(c) shows the distributions of the wall vorticity, centreline velocity and centreline disturbance intensity for different spacing ratios at Reynolds number 2000, respectively. Figure 12(a) shows that there are two peak values in wall vorticity distribution

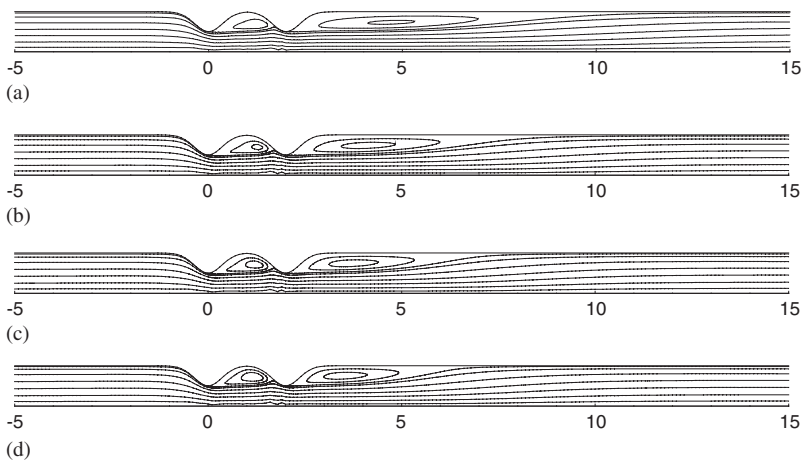

Figure 13. The streamlines of turbulent flows in the stenosed tube for different Reynolds number at $S/D = 1$: (a) Re = 500; (b) Re = 1000; (c) Re = 2000; (d) Re = 4000.

both of which occur slightly upstream of the two throats, respectively. The peak value of wall vorticity generated by the first stenosis is always greater than that generated by the second stenosis. However, the downstream peak wall vorticity grows up with S/D increasing. When S/D reaches 4, the peak wall vorticity near the second stenosis nearly recover to the same value as that near the first stenosis. The recirculating eddy forming between the two stenoses results in a negative wall vorticity peak occurring proximal to the second stenosis when S/D is less than 3 while the negative wall vorticity peak does not occur proximal to the second stenosis with S/D equal to 3 or 4. From Figure 12(b), it can be seen that the maximum centreline velocity occurs slightly downstream of the stenosis because the formation of a re-circulation zone behind each stenosis reduces the cross-sectional area of the flow. Figure 12(c) presents the distribution of the centreline disturbance intensity that is given by $\sqrt{2k}$ in which k denotes the non-dimensional turbulence kinetic energy. Therefore, the disturbance intensity can be referred to as an indicator of turbulence intensity. Note that the maximum centreline disturbance intensity near the second stenosis is always higher than that near the first stenosis for all the spacing ratios. Besides, the downstream peak value of wall vorticity increases with spacing ratio increasing until the spacing ratio S/D reaches 4. It can be deduced that in this work, the double stenoses have the strongest superposed effects on the downstream flow fields when the distance between the double stenoses is 4D. Lee [11] showed that for a laminar double-stenosed flow, the first stenosis has a diminishing effect on the flow fields distal to the second stenosis with the distance between the two stenoses increasing. The characteristics of the turbulent flow fields are evidently different from those of the laminar flow fields in the stenosed tubes.

For a given spacing ratio and a constriction ratio of the second stenosis, the typical streamlines at Reynolds numbers from 500 to 4000 are shown in Figure 13. In this case, in order to study the influence of Reynolds number on the flow fields through the double stenoses, the spacing ratio and constriction ratio of the second stenosis were fixed to 1 and 0.5, respectively. Beyond Reynolds number 500, the flows distal to the stenosis are not in laminar range and therefore the length of the recirculation zone behind the stenosis become smaller

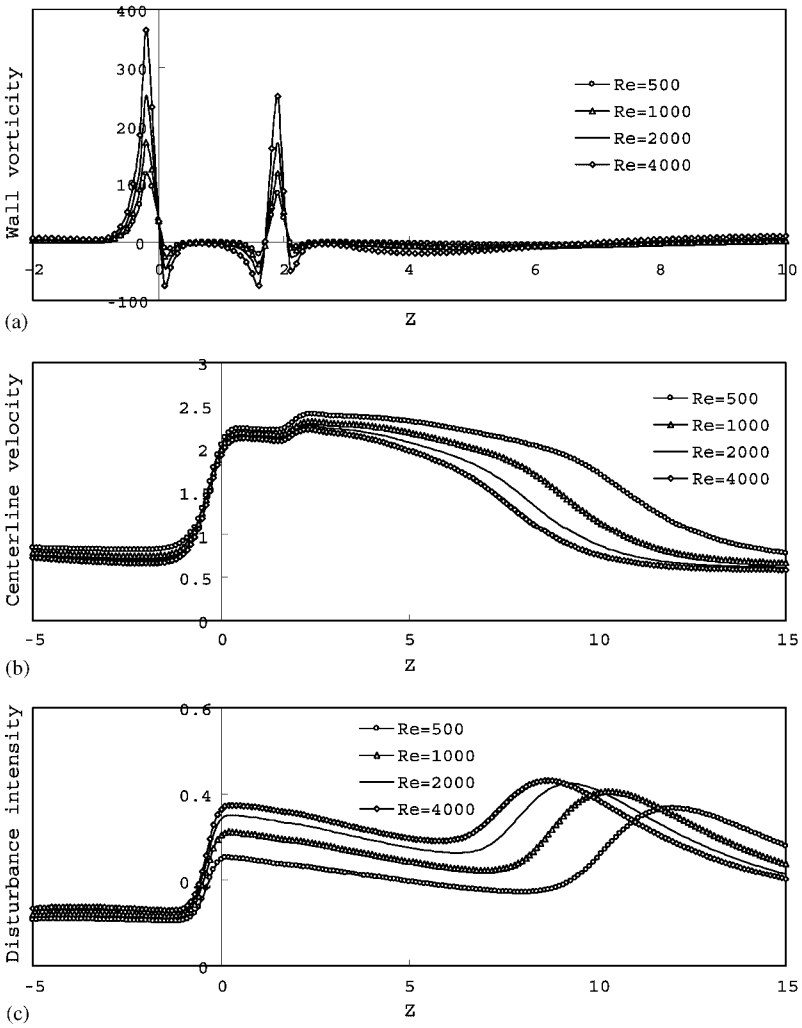

Figure 14. The flow characteristics through the double stenoses for different Reynolds numbers at $S/D = 1$: (a) wall vorticity distribution; (b) centreline velocity distribution; (c) centreline disturbance intensity distribution.

with Reynolds number increasing. A recirculation zone is full of the valley between the two stenoses for $S/D = 1$, with little changes to the separation and reattachment points as the Reynolds number is increased. From Figure 14(a), it can be seen that the two peak values of the wall vorticity grows up rapidly with the Reynolds number increasing. As mentioned previously, the peak value of wall vorticity generated by the second stenosis is usually much less than that generated by the first stenosis. Figure 14(a) shows that the differences between the two peak values of wall vorticity generated by double stenoses also increase with the Reynolds number increasing. On the contrary, it can be seen from Figure 14(b) that the value of the non-dimensional centreline velocity is slightly decreasing with the Reynolds number

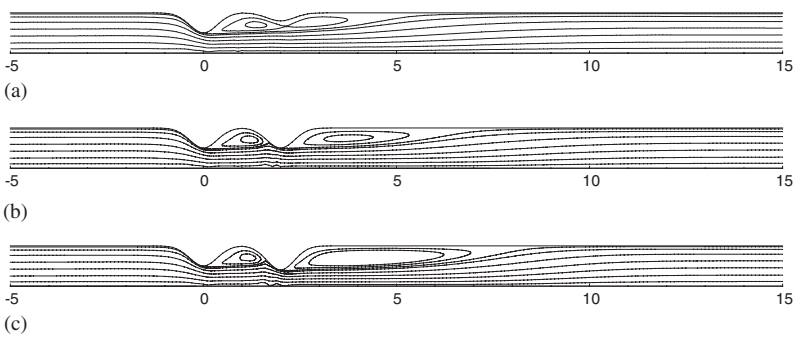

Figure 15. The streamlines of turbulent flows in the stenosed tube for different constriction ratios of the second stenosis at Re = 2000: (a) $c_2 = 0.2$; (b) $c_2 = 0.5$; (c) $c_2 = 0.6$.

increasing. This may be due to two reasons one of which is that in transitional or turbulent flows, the higher Reynolds number can lead to a smaller recirculation zone distal to each stenosis that has less effect on the cross-sectional area of the flow. Another reason is that the fully developed turbulent flow for the higher Reynolds number has the blunter velocity profiles in the cross sections of the flow. Figure 14(c) shows that the peak value of the centreline disturbance intensity goes up with the Reynolds number increasing. Besides, it can be noticed that the distance between the location of peak disturbance intensity downstream of the stenosis and the stenosis decreases with the Reynolds number increasing.

With c_1 set to 0.5, the characteristics of the recirculation eddy formed downstream of each stenosis were studied with the constriction ratio c_2 of the second stenoses varying from 0.2 to 0.6. In this case, the spacing ratios and Reynolds numbers were fixed to 1 and 2000, respectively. Figure 15 presents the streamline distribution for different constriction ratios. Figure 16(a), 16(b) and 16(c) shows the wall vorticity, centreline velocity and centreline disturbance intensity for different constriction ratios of the second stenoses, respectively. From Figure 15, it was observed that for $c_1 = 0.5$ and $c_2 = 0.2$, the circulation eddy between the two stenoses spread beyond the second stenosis, merging with the eddy that formed behind the second stenosis. This flow phenomenon has a significant influence of the downstream wall vorticity characteristics. Usually the peak wall vorticity near the stenosis should be much more than zero. When $c_2 = 0.2$, however, the peak wall vorticity near the second stenosis does not appear and the corresponding value is unexpectedly less than zero. It can be found from Figure 16(a) that the peak wall vorticity caused by the second stenosis is lower than that caused by the first stenosis when $c_2 \leqslant c_1$. In contrast, the peak wall vorticity generated by the second stenosis with $c_2 = 0.6$ increases dramatically and is much higher than that generated by the first stenosis with $c_2 = 0.5$. From Figure 16(b), it can be seen that the peak centreline velocity distal to the second stenosis with $c_2 = 0.6$ is also much higher than those distal to the second stenosis with $c_2 = 0.5$ and 0.2. The same trend can be observed in the profiles of the centreline disturbance intensity distribution in Figure 16(c). At the same time, it can be found that the differences between the flow behaviour for $c_2 = 0.5$ and that for $c_2 = 0.2$ are not so large although the difference of the corresponding cross-sectional areas between $c_2 = 0.5$ and 0.2 is much larger than that between $c_2 = 0.5$ and 0.6. Therefore, it can be concluded that $c = 0.5$ can be selected as the accepted critical value of stenosis that is the degree of vessel block beyond which there are abrupt changes in the flow properties. Actually, for artery

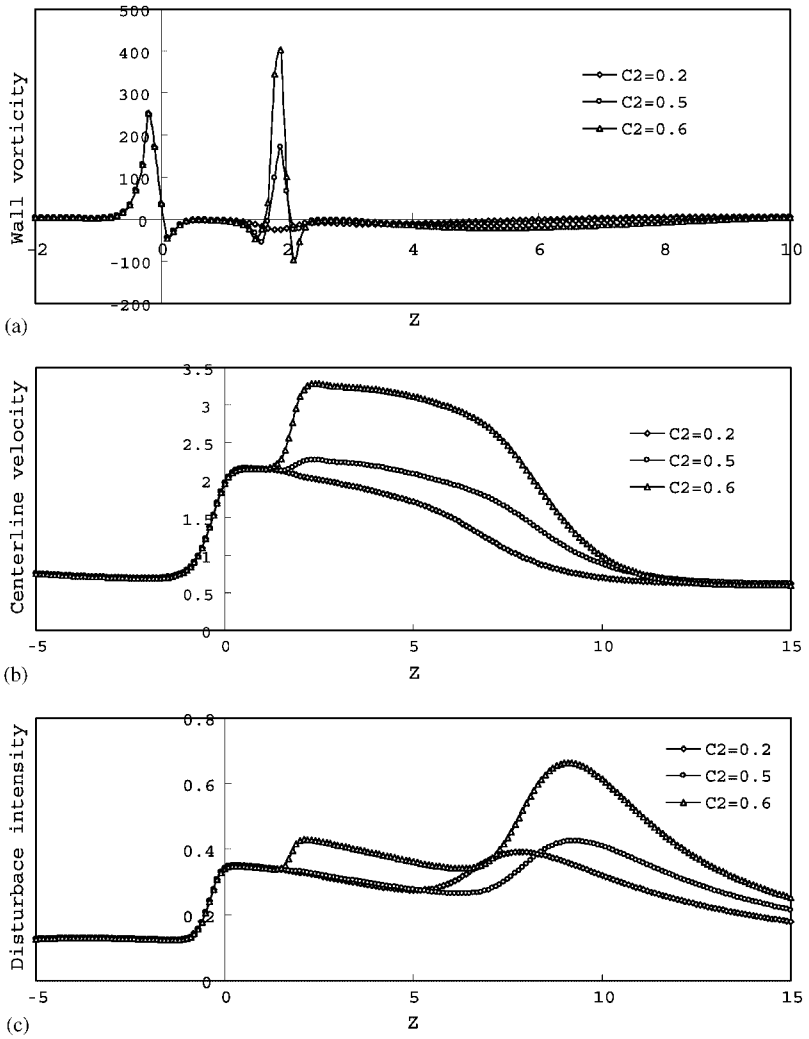

Figure 16. The flow characteristics through the double stenoses for different constriction ratios at Re = 2000: (a) wall vorticity distribution; (b) centreline velocity distribution; (c) centreline disturbance intensity distribution.

disease, the clinic treatment is often based on whether the artery is more than 75% stenotic which corresponds to $c = 0.5$.

With both c_1 and c_2 set to 0.5, the reattachment points of the recirculation eddies formed downstream of each of the stenoses for different stenosis spacing ratios are shown in Figure 17. The corresponding separation points are not shown here because there is little change for them with Reynolds number varying. In the flows through the double stenoses, a stable recirculation zone is established between the two stenoses and the location of the corresponding reattachment point almost does not change. Therefore, here we mainly focus on the recirculation zone

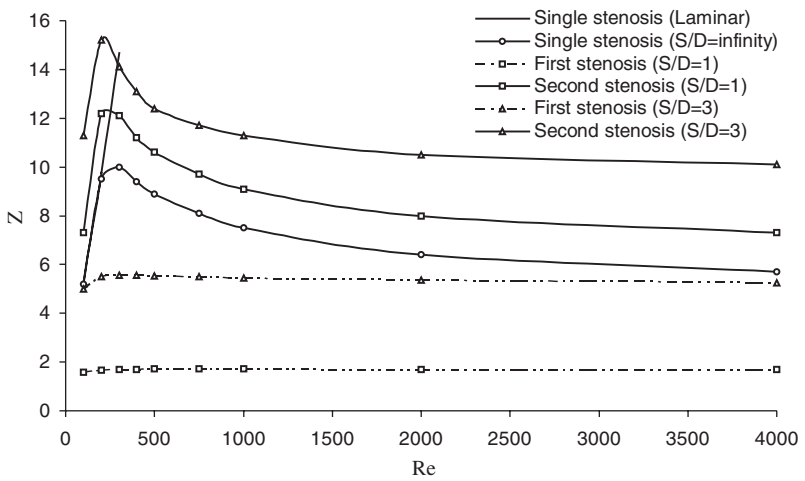

Figure 17. The locations of the reattachment points of the recirculation zones distal to the stenoses for various Reynolds numbers when $c_1 = c_2 = 0.5$.

distal to the second stenosis or distal to the single stenosis. Figure 17 shows the variation of the reattachment points with the Reynolds number when S/D is set to 1, 3 and ∞. The prediction by laminar-flow modelling is also plotted in this figure with the Reynolds number less than 300 for $S/D = \infty$. Again the excellent agreement is found between the numerical predictions by laminar-flow modelling and turbulence modelling in the laminar flow range. At the vicinity of the critical Reynolds number, the locations of reattachment points change rapidly with the Reynolds number varying. When Reynolds number is below its critical value, the flow distal to the stenosis is in a state of laminar flow and the reattachment points rapidly spread downstream as the Reynolds number increasing. When Reynolds number is larger than its critical value, the flow distal to stenosis becomes transitional or turbulent and the corresponding reattachment points rapidly move upstream until the Reynolds number reaches 1000. Beyond the Reynolds number 1000, the locations of the reattachment points do not change so evidently only with a little upstream movement. Figure 17 shows that the critical Reynolds number for the flows through single stenoses is about 300 as mentioned in the Section 5.1. In contrast, it can be observed from Figure 17 that the critical Reynolds numbers for the flows through double stenoses are much less than 300 and approach to 200. This means that the more stenoses can result in a lower critical Reynolds number and lead to an earlier occurrence of turbulence for the stenotic flows.

6. CONCLUSION

In the present study, we have further verified that in the laminar flow region, the numerical predictions by k–ω turbulence model matched those by the laminar flow model very well. This suggests that the k–ω turbulence model is not only suitable for the prediction of the low Reynolds number turbulent stenotic flow, but also suitable for the prediction of laminar flow.

Using k–ω model, we successfully predicted the critical Reynolds number at which the flows distal to a stenosis becomes transitional or turbulent.

The numerical solutions to the flow fields through double axisymmetric bell-shaped stenoses in a circular tube were obtained for a Reynolds number range 100–4000 with different constriction ratios and spacing ratios of the second stenosis. The effect of the series stenoses on flow characteristics such as streamlines, wall vorticity, centreline velocity and disturbance intensity as the flows passes through two adjacent vascular stenoses are numerically investigated. It was observed that the characteristics of the turbulent flow fields are greatly different from those of the laminar flow fields in the stenosed tubes. The extent of the spreading of the recirculation region from the first stenosis and its effects on the second stenosis depend on the stenosis spacing ratio, constriction ratio and the flow Reynolds number. The recirculation zone formed downstream of the first stenosis has a relatively weak effect on the vortex produced by the stenosis downstream with S/D increasing. However, the double stenoses have the strongest superposed effects on the distribution of turbulence intensity in the downstream region when the spacing ratio S/D reaches 4. Generally, the peak values of the wall vorticity and the centreline disturbance intensity both grow up with the Reynolds number increasing. For $c_1 = 0.5$ with $c_2 \leqslant c_1$, the maximum value of wall vorticity generated by the second stenosis is always less than that generated by the first stenosis. However, the maximum centreline velocity and disturbance intensity at the second stenosis are higher than those at the first stenosis. In contrast, for $c_1 = 0.5$ with $c_2 = 0.6$, the maximum values at the second stenosis are dramatically higher than those at the first stenosis whether for centreline velocity and disturbance intensity or for wall vorticity. The present study shows that the more stenoses can result in a lower critical Reynolds number that means an earlier occurrence of turbulence for the stenotic flows.

REFERENCES

1. Roach MR. Poststenotic dilatation in arteries. *Cardiovascular Fluid Dynamics* 1972; **2**:111–139.
2. Ku DN. Blood flow in arteries. *Annual Review of Fluid Mechanics* 1997; **29**:399–434.
3. Clark C. Turbulent velocity measurements in a model of aortic stenosis. *Journal of Biomechanics* 1976; **9**: 677–687.
4. Deshpande MD, Giddens DP. Turbulence measurements in a constricted tube. *Journal of Fluid Mechanics* 1980; **97**:65–89.
5. Saad AA, Giddens DP. Velocity measurements in steady flow through axisymmetric stenoses at moderate Reynolds numbers. *Journal of Biomechanics* 1983; **16**:505–516.
6. Wilcox DC. *Turbulence Modeling for CFD*. DCW Industries, Inc.: Boston 1993 and 1998.
7. Deshpande MD. Steady laminar and turbulent flow through vascular stenoses models. *Ph.D. Thesis*, Georgia Institute of Technology, 1977.
8. Ghalichi F, Deng X, Champlain AD, Douville Y, King M, Guidoin R. Low Reynolds number turbulence modelling of blood flow in arterial stenoses. *Biorheology* 1998; **35**:281–294.
9. Wilcox DC. Reassessment of the scale-determining equation for advanced turbulence models. *AIAA Journal* 1988; **26**:1299–1310.
10. Wilcox DC. Simulation of transition with a two-equation turbulence model. *AIAA Journal* 1994; **32**:247–255.
11. Lee TS. Numerical studies of fluid flow through tubes with double constrictions. *International Journal for Numerical Methods in Fluids* 1990; **11**:1113–1126.
12. Lee TS. Steady laminar fluid flow through variable constrictions in vascular tubes. *Journal of Fluids Engineering, ASME* 1994; **116**:66–71.
13. Damodaran V, Rankin GW, Zhang C. Numerical study laminar flow through tubes with multiple constrictions using curvilinear co-ordinates. *International Journal for Numerical Methods in Fluids* 1996; **23**:1021–1041.
14. Lee TS, Liao W, Low HT. Development of an artificial compressibility methodology with implicit LU-SGS method. *International Journal of Computational Fluid Dynamics* 2001; **15**:197–208.

15. Lee TS, Liao W, Low HT. Turbulence modelling using artificial compressibility with implicit LU-SGS method. *Proceedings of the International Conference on Computational Fluid Dynamics*, vol. 2, Sydney, Australia. Springer: Berlin, 2002.
16. Chorin AJ. A numerical method for solving incompressible viscous flow problems. *Journal of Computational Physics* 1967; **2**:12–26.
17. Michelassi V, Martelli F. Efficient solution of turbulent incompressible separated flows. *Notes on Numerical Fluid Mechanics* 1990; **29**:373–390.
18. Roe PL. Approximate Riemann solvers, parameter, vectors, and difference schemes. *Journal of Computational Physics* 1981; **43**:357–372.
19. Mansour NN, Kim J, Moin P. Reynolds-stress and dissipation rate budgets in a turbulent channel flow. *Journal of Fluid Mechanics* 1988; **194**:15–44.
20. Zijlema M, Segal A, Wesselinh P. Finite volume computation of 2D incompressible turbulent flows in general co-ordinates on staggered grids. *International Journal for Numerical Methods in Fluids* 1995; **20**:621–640.
21. Rastogi AK. Hydrodynamics in tubes perturbed by curvilinear obstructions. *Transactions*, ASME 1984; **106**: 262–269.
22. Melaaen MC. Analysis of fluid flow in constricted tubes and ducts using body-fitted non-staggered grids. *International Journal for Numerical Methods in Fluids* 1992; **15**:895–923.
23. Yongchareon W, Young DF. Initiation of turbulence in models of arterial stenoses. *Journal of Biomechanics* 1979; **12**:185–196.

